IAC–19–B4.6A.4

ADCS conceptual design for GoSolAr demonstrator mission

Mr. Jose Luis Redondo Gutierrez
German Aerospace Center (DLR), Germany, Jose.RedondoGutierrez@dlr.de

Mr. Ansgar Heidecker
German Aerospace Center (DLR), Germany, ansgar.heidecker@dlr.de

Dr. Patric Seefeldt
German Aerospace Center (DLR), Germany, Patric.Seefeldt@dlr.de

Dr. Jian Guo
Delft University of Technology (TU Delft), The Netherlands, J.Guo@tudelft.nl

This paper aims to provide a detailed analysis of the preliminary Attitude Determination and Control System (ADCS) design of DLR's (German Aerospace Center) demonstrator mission GoSolAr (Gossamer Solar Array). The goal of this mission is to demonstrate the two-dimensional deployment of a $25m^2$ flexible solar array in orbit. Understanding of the satellite configurations and control phases is critical for the design of the ADCS. The main structural configurations are stowed and deployed, in which the satellite consists of a central part to which the solar array is attached via four composite booms. The control phases are detumbling, deployment and acquiring and maintaining an orientation w.r.t. the Sun.
This study focuses in developing a control approach for the attitude of the satellite able to deal with the difficulties inherent to the GoSolAr satellite.These difficulties can be divided in two groups, related with the particularities of the deployed structure and to the limitations of the attitude actuators selected. In relation with the structure, the most concerning issues are related with the considerably high area-to-mass and moment of inertia-to-mass ratios, which increase the effect of external disturbances and reduce that of the control actuators. This initial design contains only magnetorquers, generating a locally underactuated system.
The analyses focuses in the pointing phase, which aims to reach and maintain a relative orientation of the main axis of inertia w.r.t. the Sun, while generating a spin around this axis to stabilize the satellite. In relation to this phase, two control approaches are explained, implemented and evaluated. The first one is based on using a linearization of the plant combined with an LQR (linear-quadratic regulator) approach. The second control approach is known as the Udwadia-Kalaba approach, and is based in the parallelism between constrained and controlled systems. This approach leads to a non-linear controller which can include complex guidance instructions.
The performance of these controllers is evaluated for the nominal case, confirming that they are able to fulfill the requirements. The difference in performance between LQR and Udwadia-Kalaba control approaches is explained, focusing on convergence time and long term error. Finally, some limitations in relation to the ADCS design are pointed out, related to control actuation limitations and to assumptions made when deriving the controllers. In relation to the control actuation, the use of magnetorquers imposes a limitation in altitude and in orbital inclination. The potential consequences of neglecting the flexibility are also addressed qualitatively.
keywords: ADCS, Control, LQR, Udwadia-Kalaba, GoSolAr,

Nomenclature & Abbreviations

Abbreviations

ADCS Attitude Determination and Control Subsystem

ACS Attitude Control Subsystem

DLR German Aerospace Center

FDIR Failure Detection, Isolation and Recovery

GoSolAr Gossamer Solar Array

LEO Low Earth Orbit

LQR Linear-Quadratic Regulator

UK Udwadia-Kalaba

Nomenclature

b Magnetic field

I Moment of inertia

L Angular momentum

m Magnetic dipole

q Quaternion

r Position

w Sun vector

T Torque

ω Angular rate

1. Introduction

This paper introduces the initial design of the ADCS (Attitude Determination and Control Subsystem) for the DLR's (German Aerospace Center) mission GoSolAr (Gossamer Solar Array). This mission aims to deploy a structure consisting in a flexible solar array in LEO (Low Earth Orbit) as illustrated in figure 1. This study focuses in particular on the

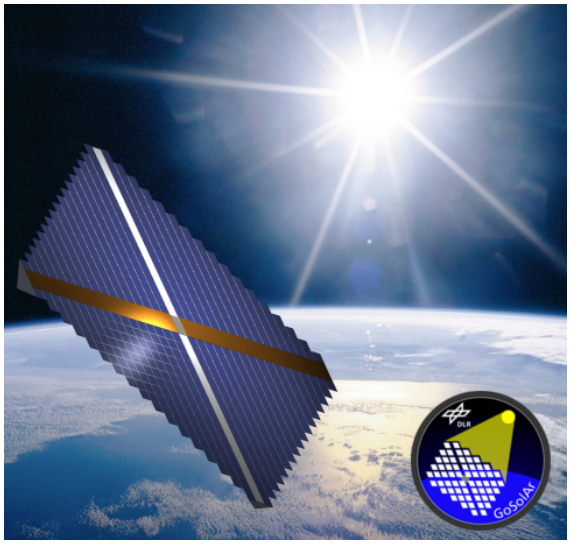

Fig. 1: Artist's impression of the GoSolAr satellite.

design of the ACS (Attitude Control Subsystem), developing and analyzing the performances of several attitude controllers [9].

The remainder of this section introduces the benefits of using this kind of structures in space as well as the main challenges that it introduces in relation to attitude control and explains the structure of the rest of the paper.

1.1 *Deployable structures*

The potential of deployable light-weighted structures in space is driven by two main factors:

1. miniaturization of satellites and their components and
2. technological advances in key related areas, e.g. ultralight composite booms [19].

These structures have two main advantages w.r.t. conventional compact satellites:

- High area-to-mass ratio. The deployed structure does not need to sustain the launch phase and therefore the structural components can be considerably reduced. This leads to a decrease in the area-to-mass ratio of 1 to 2 orders of magnitude. It is a considerable advantage in the sense that it decreases the launching cost for applications that require large areas (e.g. communication antennas and solar sailing).
- Low launching volume. As the structure is launched stowed, the volume it occupies is considerably lower than that of the final deployed satellite. This is also a benefit regarding launching costs.

There are many potential areas in space for deployable structures, such as solar and drag sailing. Solar sailing consist of using a big reflective area to transfer the momentum of solar radiation to a satellite. An example of a demonstrator mission that includes flexible phtovoltaic as well as components required for solar sailing is JAXA's mission IKAROS [15]. A drag sail consists of a deployable membrane that increases the drag area of a satellite in order to dissipate orbit energy when interacting with the residual atmosphere in a low orbit. It is considered a solution for the emerging problem of LEO orbits saturation [5].

Even though the charateristics of the structure of the GoSolAr satellite is relatively similar to the structures used in those two areas, the objective is considerably different. The aim is not to change the momentum of a satellite but rather to allow having a bigger solar array with a lower weight, increasing the power available per kg allocated to this subsystem.

NASA's mission ROSA [2] is in line with this objective.

These structures have some particularities that are considerably challenging for the ADCS. Most of these challenges are caused by the increase in area-to-mass ratio. The increase in this ratio increases also the moment of inertia-to-mass ratio. Increasing moment of inertia and area makes the spacecraft more susceptible to external disturbances. The effect of solar radiation and drag is linked to the area and the effect of the gravity gradient to the moment of inertia. Further more, depending on the relative location of the center of mass and the center of pressure, high disturbance torques can appear. Conventional actuators, such as thrusters and reaction wheels, are usually confined in the volume of the stowed structure. This draws a limit in their size and in the arm w.r.t. the center of mass, limiting considerably their actuation capability. Additionally, the increase in the moment of inertia increases the angular inertia, requiring higher actuation torques to achieve the same effect.

There are some solutions targeting these problems, mainly based on controlling the shift between the center of pressure and the center of mass, using either additional moving surfaces or additional moving masses, see e.g. [6]. However, these actuators are still in an early stage of their technological development. Therefore, in the GoSolAr mission the aim is to control the attitude of the satellite limiting ourselves to conventional actuators.

1.2 *Sectional organization of the paper*

The paper is organized as follows. It starts giving a brief explanation of the GoSolAr mission in section 2. This explanation includes the main objectives of this mission, some comments of the technological developments it contributes to and an analysis of the requirements related to the ADCS. In section 3 the simulation environment that is used to test the performance of each controller is explained. Section 4 dives into the two phases of the mission we are developing attitude controllers for: detumbling and controlled attitude. For each of the phases a control approach (or multiple ones for the case of the controlled attitude phase) is briefly introduced from a theoretical perspective and applied over the GoSolAr mission. In section 5 each controller is studied for the nominal case and some limitations are pointed out. The main conclusions and some ideas for future work are included in section 6. The appendix includes relevant data regarding the GoSolAr satellite.

2. GoSolAr demonstrator mission

GoSolAr is a DLR's demonstrator mission that focuses in the gossamer deployment of thin film photovoltaic arrays [8]. Two objectives are derived from this goal:

1. Development of a deployment technology for a 25 m^2 solar array.

2. Development of a flexible photovoltaic membrane.

The satellite consists of a central rigid body to which four composite booms are attached. The solar array is fixed to the central body and to the tip of each boom, as can be observed in figure 2. GoSolAr inherits knowledge and technology from previous DLR's projects which used similar deployable structures, including GOSSAMER-1 [12] and ADEO [13]. It is designed as a payload for a technology demonstration in a low Earth orbit. In the mission two different configurations and one intermediate configuration is present. This is shown in Figure 2. At first the satellite is in the stowed configuration for launch. This compact configuration is about 500 mm × 500mm × 500mm big and has a weight of about 50 kg. The deployment is then carried out in two steps, one for each dimension of the membrane.

Two different types of photovoltaic shall be demonstrated and it is required to size the array so that each type can generate a power 140 W in order to properly demonstrate the capability to power a small satellite bus. Due to limitations in resources and available infrastructure the maximum size is limited 5 mx5 m. Currently products of two manufactures for Copper Indium Gallium Selenide (CIGS) photovoltaic technologies, as shown in Figure 3, are under investigation. More information regarding the satellite can be found in [14].

In the following subsections a small overview on the GoSolAr mission and a possible attitude determination and control subsystem is given. This is followed by an explanation on the main ADCS requirement and a detailed description of the components of this subsystem.

2.1 *Mission overview*

As a technology demonstrator GoSolAr will probably fly with a small satellite bus piggy-back to a Low Earth Orbit. A lot of missions are launched to a Sun Synchronous Orbit with an orbit inclination of about 97° and in altitudes between 550 km and

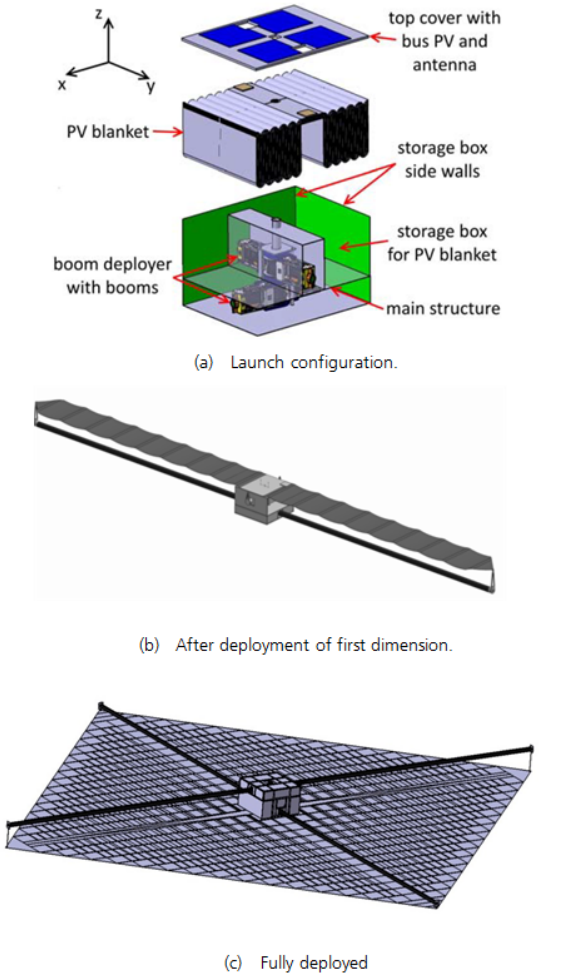

(a) Launch configuration.

(b) After deployment of first dimension.

(c) Fully deployed

Fig. 2: GoSolAr configurations.

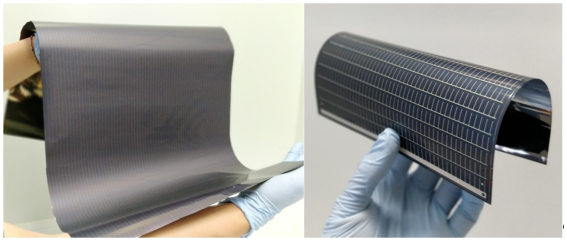

Fig. 3: Flexible CIGS modules; Left: Flisom; Right: Ascent Solar.

720 km.Therefore the current design takes these orbit range into account.

The mission is designed to be carried out in eight phases as shown in Figure 4.

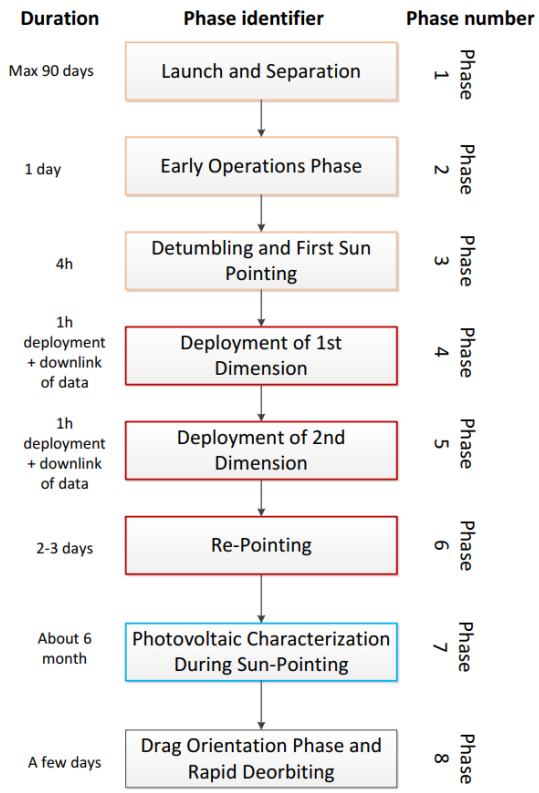

Fig. 4: GoSolAr mission phases.

The mission phases are briefly described in the next sections, already taking some of the later presented analysis results into account.

2.1.1 *Launch and Separation*

During launch and separation from the launcher the spacecraft is in stowed configuration as shown in Figure 2 (a). At separation the spacecraft is activated. After the bus system is operational, the GoSolAr payload will be activated by the bus system by ground command. This phase shall be less than 90 days in order to avoid long-term storage effects.

2.1.2 *Early Operation Phase*

During this phase the initial boot process of the spacecraft and the GoSolAr payload takes place. The spacecraft remains in stowed configuration. The payload board computer (PBC) is booted. This is done in a stepwise incremental procedure to allow close spacecraft control and FDIR in case of non-nominal

behaviour. Sensor data will be read out including first camera pictures. Status information and test images will be downlinked. This phase is expected to be covered with one or two ground-contacts. The number of required ground contacts depends on the amount of data that is to be downlinked. The phase requires about one day.

2.1.3 *Detumbling and first Sun Pointing*

After separation from the upper stage, the satellite is tumbling. From other missions, it is estimated that the tumbling rate is about 12 deg/s about a random axes (several Montecarlo runs were per-formed). After the detumbling the satellite is set into spin about the deployment plane normal. After this spin stabilization, the satellite is pointed sunwards.

2.1.4 *Deployment of 1st Dimension*

The deployment of the first dimension will take about 30 to 46 minutes depending on the chosen drive system. The deployment will last longer than one ground contact. Regarding operations it has to be assumed that the system will have to be controlled and operated with one ground station only (Weilheim) and that real time monitoring with several ground station will not be funded.

In a first step the Hold Down and Release Mechanisms (HDRM), which keep the system in a mechanically stable launch configuration, needs to be released. Afterwards a system check out will be performed and sensor data will be downlinked.

Then, if no failure occurs, the motor for the first direction of the deployment is turned on but without rotating. After another system check out the deployment is started via time tagged command to ensure that deployment starts in sunlight and early enough before the next downlink such that nominal deployment of the first dimension will be done just a few minutes before the actual ground contact.

In case of non-nominal behaviour, the system autonomously stops the deployment (emergency stop) and transits into a safe mode. Such emergency stop data packages plus corresponding historical data is subsequently downlinked with first priority at the next ground contact. In nominal case, the deployment will stop at the nominal deployment's end position.

The phase ends with complete system check out and downlink of sensor data including pictures from the deployment process.

2.1.5 *Deployment of 2nd Dimension*

The deployment of the second dimension will also take 30 to 46 minutes depending on the chosen drive system. Again it will not be possible to have a real time monitoring of the deployment process.

The motor for the deployment of the second dimension is turned on but without rotating. After another system check out is made the deployment can be started. The deployment is started via time tagged command to ensure that also the deployment of this dimension starts in sunlight and sufficiently well before the next downlink such that nominal deployment of the first dimension will be done a few minutes before the actual ground contact.

In case of non-nominal behaviour, the system autonomously stops the deployment (emergency stop) and transits into a safe mode. Emergency stop data packages plus corresponding historical data is subsequently downlinked with first priority at the next ground contact. In nominal case, the deployment will stop at the nominal deployment's end position.

The phase ends with complete system check out and downlink of sensor data including pictures from the deployment process.

2.1.6 *Re-Pointing*

After deployment, due to disturbances in orbit and slight asymmetries of the system, it is likely that a shorter period of a few orbits is required to re-point GoSolAr again to the sun. Ideally, the angular momentum would be maintained, leading to the deployed configuration already spinning and pointing towards the sun without further actuations. However, non-symmetrical configurations might appear throughout the deployment, leading, by interaction with external disturbances, to changes in the pointing axis and the angular rate. Therefore, it will be necessary to stabilize the deployed spacecraft again, correct spin axis and spin rate again and to re-point the space craft towards the Sun again.

2.1.7 *Photovoltaic Characterization During Sun-Pointing Phase*

The attainable pointing accuracy depends mainly on two external factors:

- density of the atmosphere and
- magnetic field evolution throughout the orbit.

The density of the atmosphere becomes a problem for attitude control when it is more than $1.5 \cdot 10^{-12}\,\mathrm{kg/m^3}$, corresponding to different altitudes depending on the solar activity. It also depends also

on the ballistic coefficient of the object. Above this value the pointing requirement is not achievable with the currently foreseen attitude control system. This ultimately limits the possible duration of this phase.

Regarding time scales, it is of importance that characterization of a single Generator is done in a few seconds while the characterization of the complete solar array can take a few minutes. So in both cases the related time scale is short in comparison to the time scales of any pointing activity, e.g. slewing.

Independently of the pointing accuracy, the accuracy of knowledge of actual (even transient) pointing is usually much better. For a simple attitude determination and control system, as discussed in the present context, the accuracy of knowledge of attitude would be in the order of 0.5°.

Bringing these three aspects (slow slew rate compared to characterization measurement, and knowledge of pointing always much better than 10°) together, it is possible to perform characterization of photovoltaic throughout any attitude control manoeuvres.

2.1.8 *Drag Orientation Phase and Rapid Deorbiting*

During the last days of the mission, well below the altitude linked to the previously mentioned critical density limit, the orientation of the sail will be determined by drag, as the attitude control system at such altitudes will not be able to counteract the drag disturbance. Still this time could be used for some additional measurement with the photovoltaic in very low orbits.

2.2 *Attitude determination and control subsystem*

The main ADCS requirement of the mission is driven by the need of characterizing the behaviour of the solar array, thus controlling its orientation towards the sun. This requirement consists of reaching and maintaining a relative orientation w.r.t. the sun with an accuracy of 10 deg. Other requirements that are related to the ADCS are:

- To ensure safe deployment of the solar array.
- Deorbiting time. Due to the membrane-like structure, the orientation of the satellite w.r.t. the atmosphere has an extremely high influence in the drag and, thus, in the deorbiting time. The minimum deorbiting time is defined as 6 months and the maximum as 25 years.

From an ADCS perspective the mission can be divided in the following phases:

- Launch. This phase is considered out of the scope of this paper. It ends with known (to a certain accuracy) position and velocity and unknown attitude and angular rate. The angular rate at this point is assumed to be limited to 12 deg/s.
- Detumbling. In this phase the angular rate of the satellite is reduced.
- Deployment. The deployment is conducted in two steps, one per dimension. This phase is considered out of the scope of this paper, due to the highly non-linear character of its dynamics.
- Controlled attitude. This phase consists in acquiring a desired orientation w.r.t. the sun.

The hardware components of the ADCS subsystem can be classified in sensors and actuators. The sensors give measurements that enable to estimate the attitude and angular rate of the satellite. To estimate the attitude three sets of sensors are used: coarse sun sensors, providing a complete field of view, fine sun sensors, covering the area of interest (i.e. the orientation of the solar array) and magnetometers. These sensors allow to estimate the sun vector and the magnetic field, both in a reference frame fixed to the satellite. The GPS measurements allow to compute these vectors in an inertial reference frame. Combining the information in both reference frames (e.g. using a TRIAD algorithm [3]) leads to an estimation of the attitude of the satellite. The angular rate is measured using gyroscopes, which give a direct measurement over it. The estimation of the angular rate is also used to propagate the attitude of the satellite in the absence of a measurement of the sun vector, i.e. during eclipses. The only actuators used are magnetorquers. The decision of using only this actuator is based on its price, weight and simplicity.

3. Simulation environment

In order to analyze the behavior of the satellite throughout the different phases studied, it is necessary to build a simulation environment. This section gives an explanation of the assumptions made when building this simulation environment.

Regarding the hardware of the ADCS, the sensors are assumed to be ideal. Therefore there are no noises or biases and no estimator is built. The magnetorquers are modeled having a time constant, modeling the dynamic behavior of the generated dipole, and a duty cycle, which consists of switching on and off

the actuator to be able to measure the surrounding magnetic field.

The satellite is modeled as a rigid body and the simulation is run with 6 degrees of freedom (position and attitude). However, as the focus of the paper is the ADCS, only the equations of motion related to the angular motion are shown here. These equations will be later used to derived the attitude controllers. More detailed derivations of the equations shown below can be found in [18].

Assuming a constant moment of inertia, the dynamics of the spacecraft can be derived from the angular momentum (L) as

$$\begin{aligned} L &= I\omega \\ \frac{dL}{dt} &= T - \omega \times L = I\frac{d\omega}{dt} \\ \dot{\omega} &= I^{-1}(T - \omega \times (I\omega)) \end{aligned} \quad [1]$$

where ω is the angular rate, I the moment of inertia and T the external torque.

The kinematics of the satellite are modeled using Euler symmetric parameters, which express the attitude using a quaternion. This quaternion contains information regarding the Euler axis ($[e_1, e_2, e_3]$) and angle (ϕ) (see equation 2).

$$q_{1,2,3} = e_{1,2,3} sin\frac{\phi}{2}; \quad q_4 = cos\frac{\phi}{2}; \quad [2]$$

This formulation leads to expression 3 for the kinematics of the system, where q is the quaternion and $\tilde{\omega}$ is the extended angular rate. To convert ω into $\tilde{\omega}$ a forth component equal to zero is added. Additionally, a constraint ensuring the that the norm of the quaternion remains unitary was added. More information about quaternion algebra (e.g. quaternion product) can be found in [11].

$$\dot{q} = \frac{1}{2} q\tilde{\omega} \quad [3]$$

The decision of leaving the flexibility of the structure out of the analysis is driven by the complexity of modeling the behavior of the resulting flexible body. However, initial analyses showed that the natural frequencies of the structure do not overlap with the frequencies of the external disturbances or with the actuators frequencies. Therefore, if the control frequency is defined such as that it does not interact with the structure frequencies, it can be avoided to excite these frequencies. Further analyses will be conducted in this area.

In relation to the external forces and torques accounted for, the following sources are considered: gravity field, magnetic field, atmosphere and radiation pressure. The torque generated due to the gravity is shown in expression 4, where I is the moment of inertia, μ Earth's gravitational constant, r the position vector and r_u the unitary position vector.

$$T_g = 3\frac{\mu}{|r|^3}(r_u \times (Ir_u)) \quad [4]$$

The torque due to the external magnetic field is shown in expression 5, where m is the satellite magnetic dipole and b the intensity of the magnetic field.

$$T_m = m \times b; \quad [5]$$

The solar pressure is computed as shown in equation 6.

$$f_r = i_r((1 - C_{sr})\vec{s} + 2(C_{sr} cos\theta + \frac{1}{3}C_{dr})\vec{n})Acos\theta; \quad [6]$$

In this expression $\vec{s}$ is the sun vector, $\vec{n}$ the normal of the surface, θ the angle between both vectors, C_{sr} the spectral reflectivity coefficient, C_{dr} the diffusive reflectivity coefficient and A the area. The solar irradiance i_r is assumed constant with a value of 1358 W/m^2, neglecting variations related to the time of the year and the solar cycle. The resulting torque and force are computed assuming a rigid body and neglecting the influence of projected shadows between the different components of the structure.

The drag is computed using equation 7.

$$f_d = -\frac{1}{2} C_D \rho v^2 A cos\theta \frac{\vec{v}}{v}; \quad [7]$$

In this equation C_D is the drag coefficient, ρ the atmospheric density, v the velocity relative to the atmosphere, A the area and θ the angle between the normal of the area and the velocity vector. The velocity w.r.t. the atmosphere is assumed equal to the orbital velocity. The atmospheric density is computed only once at the beginning of the simulation (initial altitude) based on the Harris-Priester model [10]. Therefore daily, yearly and solar cycle-related variations are neglected. The value assumed for the F10.7 cm flux level is 111 $W/m^2/Hz$. The resulting torque and force are computed using a rigid structure.

4. Control approach

In this study attitude controllers for two mission phases (detumbling and controlled attitude) are developed. The detumbling phase aims to damp the satellite's angular rate. In the controlled attitude phase the objective is to point the solar array towards

the sun. In order to obtain a more stable configuration the satellite spins around the axis normal to the plane of the solar array and this axis is pointed along the sun vector.

This section introduces the approach followed for the detumbling phase and two alternative approaches for the controlled attitude phase.

4.1 *Detumbling*

The controller used for this phase is known as the b-dot controller [1]. This controller only needs an estimation of the magnetic field, provided by the magnetometers, and actuates using the magnetorquers. It aims to generate a magnetic dipole that opposes to the variation of the magnetic field in the reference frame fixed to the satellite. The variation of the magnetic field in inertial reference frame is assumed negligible for the time range the attitude controller works on. Therefore, minimizing the time derivative of the magnetic field in the satellite-fixed reference frame is equivalent to minimizing the angular rate between that reference frame and the inertial reference frame.

The final algorithm expresses the magnetic dipole (m) to be generated as a function of the variation of the direction of the magnetic field $\dot{\vec{b_u}}$ and a constant k_ω (see equation 8).

$$m = -k_\omega \dot{\vec{b_u}} \quad [8]$$

4.2 *Controlled attitude*

This phase is more challenging from an attitude control perspective. Therefore, two controllers have been developed. The first one is a linear-quadratic regulator (LQR), based on optimal control. The second one is a non linear approach based on the work of Udwadia and Kalaba [17]. Both approaches are first briefly introduced from a theoretical perspective and then applied to the particular case of study.

4.2.1 *Orientation w.r.t. the sun - LQR approach*

A detailed explanation of the theoretical basis of this control approach can be found in [7]. A brief introduction to its main characteristics is shown here. The derivation of the LQR controller is done in two steps: 1) linearize the equations of motion and 2) minimize the cost function.

The linearization leads to a linear system as the one shown in equation 9, where x denotes the state vector, u the control command and A and B are constant matrices defined for a particular linearization point. In this particular case the equations of motion linearized assume a rigid body and are those shown in section 3. It is important to take into account that the dynamics of the actuators are not considered in the linearization.

$$\dot{x} = Ax + Bu; \quad [9]$$

Once the linear system is defined, a cost function J is defined based on weighting matrices linked to the state vector (x) and to the control command (u). These matrices (Q,R and N) are related to the relative importance of errors in each variable and combination of variables. The controller (K) is then derived as a constant control gain which minimizes the cost function J. This optimization problem is solved with the help of the MATLAB's function *lqr*, which solves it by solving a Ricatti equation. The selection of Q, R and N was done in an iterative way, by studying the performance of the controller (K) resulting from different values of these matrices.

$$\begin{aligned} J = \int_0^\infty (x^T Q x + u^T R u + 2x^T N u) dt \\ [u = Kx]_{min(J)} \end{aligned} \quad [10]$$

The error targeted with the controller is based on direct subtraction in the case of the angular rate and in the method explained in [4] for the pointing error. This method expresses the difference between two axis that are to be aligned (according to guidance instructions). The equations resulting from its application are shown in expression 11, where v_1 and v_2 are the axes to be aligned, e the error variable and $[z\times]$ the matrix equivalent to the cross product of vector z.

$$\begin{aligned} z =& \frac{v_1 \times v_2}{|v_1 \times v_2|}; \quad \theta = arccos(v_1 \cdot v_2) \\ E =& I + sin\theta[z\times] + (1 - cos\theta)[z\times]^2 \\ e =& [E_{23} - E_{32}; E_{31} - E_{13}] \end{aligned} \quad [11]$$

The state variable used is

$$x = [e_1; e_2; \omega_1; \omega_2; \omega_3]; \quad [12]$$

and it is linearized around the point

$$x_0 = [0; 0; 0; 0; \omega_3]; \quad [13]$$

For the linearization the time derivative of the error variables e_i is assumed to be equal to ω_i. The moment of inertia is assumed diagonal. This leads to

the following expressions for matrices A and B

$$A = \begin{bmatrix} 0 & 0 & 1 & 0 & 0 \\ 0 & 0 & 0 & 1 & 0 \\ 0 & 0 & 0 & I_3\omega_3/I_1 & 0 \\ 0 & 0 & -I_3\omega_3/I_2 & 0 & 0 \\ 0 & 0 & 0 & 0 & 0 \end{bmatrix}; \quad B = \begin{bmatrix} 0 & 0 & 0 \\ 0 & 0 & 0 \\ 1/I_1 & 0 & 0 \\ 0 & 1/I_2 & 0 \\ 0 & 0 & 1/I_3 \end{bmatrix}; \quad [14]$$

The matrices chosen to define the cost function are composed of unitary matrices multiplied by 0.05 for e, 10E4 for ω and 10E5 for the commanded torque. These quantities are related both to the order of magnitude and limitations of each variable and to the control strategy. Variable e is of order 1 and ω of order 1E-2. The limitation in the dipole generated is $10A/m^2$. The control strategy is based in imposing more strict conditions for the angular rate, making sure that satellite is stably spinning. In order to follow this strategy, the weight related with errors in ω is considerably increased. As a result the cost of the commanded torque needs to be increased to avoid continuously saturating the actuators.

4.2.2 *Orientation w.r.t. the sun - U-K approach*

A theoretical explanation on this control approach can be found in [17]. It is based on the parallelism between a constraint mechanical system and a controlled mechanical system and makes use of the nowadays called Udwadia-Kalaba equation, which was proposed in the 1990's [16].

Initially we have an uncontrolled system of the form shown in equation 15, where $\ddot{q}$ is the generalized acceleration, M is the mass matrix, a the double time derivative of the state vector q and Q the sum of all internal and external forces.

$$M\ddot{q} = Q \rightarrow \ddot{q} = M^{-1}Q = a \quad [15]$$

A generic equation of motion, including the control force (Q_c) is shown in 16.

$$M\ddot{q} = Q + Q_c \quad [16]$$

A formulation of Q_c addressing a variety of constraints (or guidance instructions) is given in [17] by

$$Q_c = -Ke = M^{1/2}\left[AM^{-1/2}\right]^{+}(Aa - b) \quad [17]$$

In this equation variables A and b contain the constraints that we want to implement. These constraints can be holonomic (eq. 18) or nonholonomic (eq. 19).

$$\phi_i(q,t) = 0 \quad [18]$$

$$\psi_i(q,\dot{q},t) = 0 \quad [19]$$

Once the guidance instructions have been expressed as one of these two types, differentiating once or twice w.r.t. to time leads to the following expression

$$A(q,\dot{q},t)\ddot{q} = b(q,\dot{q},t) \quad [20]$$

from which A and b in equation [17] can be obtained. In order to deal with the variable being initially outside of the manifold described by the constraints, the intermediate terms of the time derivations are kept, generalizing the constraints to

$$\ddot{\phi} + \Sigma\dot{\phi} + \Gamma\phi = 0 \quad [21]$$

$$\dot{\psi} + \Lambda\psi = 0 \quad [22]$$

which ensures that over time the trajectory can converge but does not require that it matches exactly right from the beginning. The variables Σ, Γ and Λ are constant tuning parameters, which describe the desired convergence rates.

The control force shown in 17 minimized the cost function J shown in expression 23. However, this cost function can be generalized to that shown in expression 24, where N can be defined by the user.

$$J(t) = Q_c(q,\dot{q},t)^T\ M^{-1}(q,t)\ Q_c(q,\dot{q},t) \quad [23]$$

$$J(t) = [Q_c(q,\dot{q},t)]^T N(q,t)[Q_c(q,\dot{q},t)] \quad [24]$$

This change in the cost function is reflected in the expression of the control actuation as

$$Q_c = -N^{-\frac{1}{2}}\left[AM^{-1}N^{-\frac{1}{2}}\right]^{+}(Aa - b) \quad [25]$$

After briefly going through the formulation for this control approach, this formulation is applied to the case of study. As in the previous controller, we are using the equations of motion of a rigid body. Therefore, expression 15 can be written as

$$I\alpha = \sum T \quad [26]$$

where I is the moment of inertia, α the angular acceleration and T the different torques.

As previously mentioned, there are two main guidance instructions: 1) to spin the satellite in its main

axis of inertia and 2) align that axis with the sun vector. The first constraint can be expressed as a nonholonomic constraint as shown in 27, where ω denotes the angular rate and G denotes guidance.

$$\omega = \omega_G \quad [27]$$

The second constraint assumes that the first one is already fulfilled and is expressed as shown in 28, where s is the sun vector.

$$\omega \times s = 0 \quad [28]$$

The derivation w.r.t. time leads to an expression in line with the formulation of the controller. For the first constraint this expression is shown in equation 30, where $c_1 > 0$ is a control parameter linked to the convergence and stability of the controller.

$$\alpha + c_1(\omega - \omega_G) = 0 \quad [29]$$

When deriving the second constraint it is important to notice that there are two solutions to expression 28: both vectors can be aligned or pointing to opposite directions. In order to ensure that the controller converges to the desired point (aligned), an additional factor is added, as shown in equation 30, where $c_2 > 0$ is a control parameter linked to the convergence and stability of the controller.

$$\begin{gathered} \alpha \times s + (-1)^p c_2(w \times s) = 0 \\ w \cdot s < 0 \rightarrow p = 1; \quad w \cdot s \geq 0 \rightarrow p = 2 \end{gathered} \quad [30]$$

After these mathematical operations over the constraints, A and b in expression 17 can be computed. Regarding the cost function, the decision was made to stick to $N = M^{-1}$. After some tuning, the constant c_1 is defined as 0.1 and c_2 as 0.01.

5. Performance and limitations of the ADCS

The performance of the controllers is studied using the simulation environment explained in section 3. The nominal case for each phase is defined and each controller tested over a number of cases. Then some limitations of the controllers are pointed out and explained.

5.1 *Nominal case*

The nominal case is defined as a circular orbit of 600 km altitude, with an inclination of 97 deg and argument of perigee, right ascension of the ascending node, mean anomaly and true anomaly equal to zero. The initial date is the 1 of September of 2007.

For the detumbling phase two initial conditions are considered:

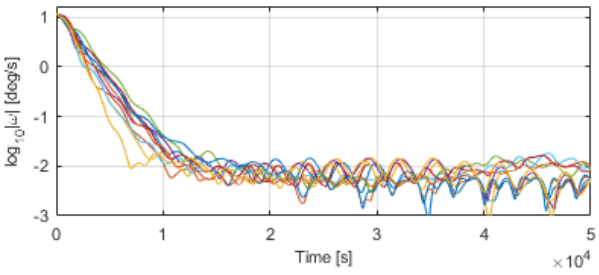

Fig. 5: Performance of b-dot controller for 10 cases. Stowed configuration.

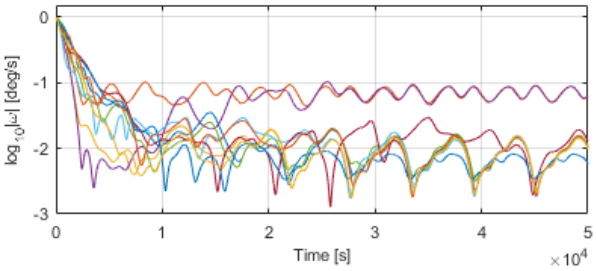

Fig. 6: Performance of b-dot controller for 10 cases. Deployed configuration.

1. Stowed satellite. Angular rate of 12 deg/s (after launch situation). Unknown attitude and angular rate direction.

2. Deployed satellite. Angular rate of 1 deg/s (potential angular rates acquired during deployment or due to other causes). Unknown attitude and angular rate direction.

For both initial conditions the objective of the controller is to reach an angular velocity equal to 0. Each initial condition is run 10 times, using uniform random distributions to compute the unknown values. The results are shown in figure 5 for case 1, and in figure 6 for case 2. These figures show the temporal evolution of the angular rate in both configurations. In order to ease the visualization, a logarithmic scale is used for the angular rate (in [deg/s]) while the time is shown in seconds.

It can be concluded that the controller is successful in both situations, achieving angular rates of less than 0.02 deg/s for the stowed scenario and less than 0.1 deg/s for the deployed one. The time needed to detumble after launch is around 3 hours.

For the controlled attitude phase the initial conditions are defined with an angular rate of 0.2 deg/s, based on the performance of the controller of the pre-

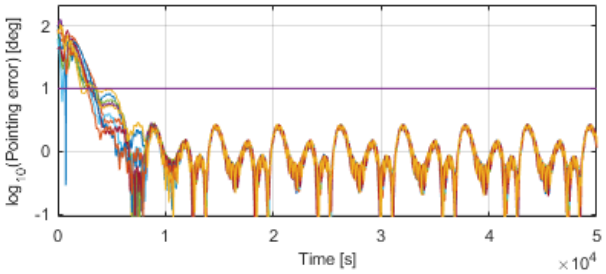

Fig. 7: Performance of the LQR controller.

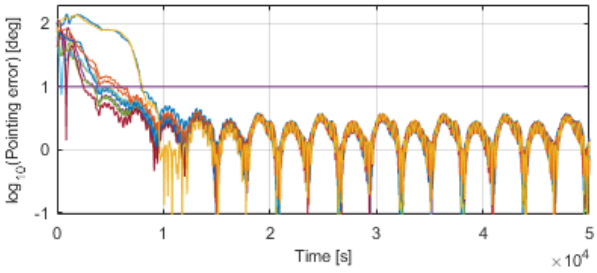

Fig. 8: Performance of the Udwadia-Kalaba controller.

vious phase. The attitude and angular rate direction are unknown. Only the deployed structure is considered. The analysis consists in running the same 10 cases for both alternatives, LQR and Udwadia-Kalaba (UK). These results are presented in figures 7 and 8. These figures show the temporal evolution of the angle between the normal to the plane containing the solar array and the sun vector (i.e. pointing error). For visualization purposes this angle is shown on a logarithmic scale. The time is given in seconds.

The accuracy obtained with the LQR controler is slightly better, but both controllers are able to fulfill the requirements of the mission. It can be seen that the performance is similar. It is also noted that the pointing error of the satellite is independent from the initial condition and its evolution is periodic and linked in frequency to the orbit.

5.2 *Limitations*

In this section two main limitations of the ADCS are explained:

- Altitude limitation.
- Local underactuation.

The limitation in altitude is related to the evolution of the magnetic field, which limit the control torque that

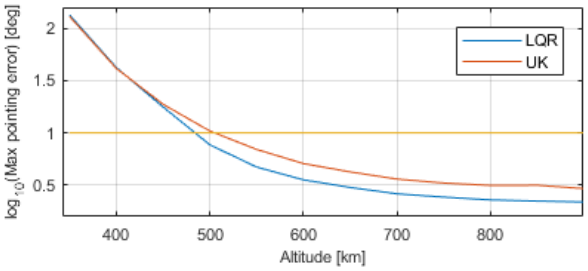

Fig. 9: Attainable accuracy depending on the altitude. F10.7 cm flux level equal to 111 $W/m^2/Hz$.

can be exerted, w.r.t. the rest of the disturbances (e.g. solar radiation or drag). The analysis includes the evolution of the pointing error for one starting case, for altitudes between 350 and 900 km. The results are shown in figure 9.

It can be seen that at orbits lower than 480-500 km the controllers are not able to comply to the requirements of the mission. This is due to the effect of drag. For determining this altitude it is important to take into account that at the F10.7 cm flux level considered (111 $W/m^2/Hz$) the atmospheric density is 1.3973E-12-1.0616E-12 kg/m^3. At other flux levels this can change. This way the altitude lower limit could be expressed as a surface depending on the flux level and the altitude. Regarding a higher limit in the altitude, none is found below 900 km.

The second limitation is the constraint of orthogonality between the control torque and the magnetic field. This condition means that the satellite is always locally underactuated. This would become a problem for orbits with low inclination where the direction of the magnetic field does not vary enough during the orbit.

6. Conclusions

The hardware developments are currently implemented on breadboard level as shown in Figure 10. It is envisaged to have a preliminary design review at the beginning of 2020.

This paper proposes a ADCS concept for the DLR's mission GoSolAr, targeting the challenges arising from the particularities of the satellite's structure and ADCS. These challenges are related to the high area-to-mass ratio and to the use of magnetorquers as the only actuators.

The attitude phases studied are detumbling and controlling the orientation w.r.t. the sun. For the first phase a b-dot controller is implemented and

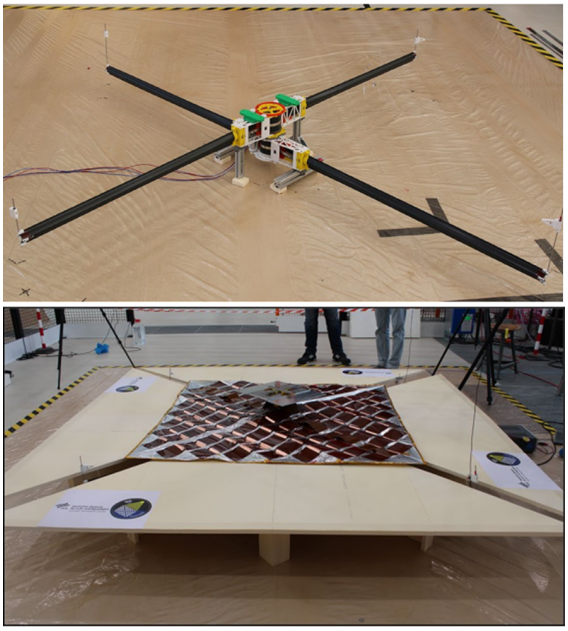

Fig. 10: GoSolAr deployment technology breadboards (1 m × 1 m. Top: only booms, Bottom: Membrane deployed with booms.

tested, being able to reduce considerably the angular rate of the satellite.

For the second phase the decision was made of spinnig the satellite around its major axis of inertia in order to obtain a more stable configuration. In this phase two algorithms are implemented, based in LQR and in the Udwadia-Kalaba approach. Both resulting controllers are able to meet the requirement of the mission, i.e. pointing accuracy of 10 deg, and are show qualitatively a similar behavior.

Further work proposed includes but is not limited to:

- Introducing a realistic model of the sensors.
- Building a filter to estimate the state vector.
- Further analysis of the flexibility of the structure and its potential interaction with the mission requirements.

References

[1] Giulio Avanzini and Fabrizio Giulietti. Magnetic detumbling of a rigid spacecraft. *Journal of guidance, control, and dynamics*, 35(4):1326–1334, 2012.

[2] Jeremy Banik, Steve Kiefer, Matt LaPointe, and Pete LaCorte. On-orbit validation of the roll-out solar array. In *2018 IEEE Aerospace Conference*, pages 1–9. IEEE, 2018.

[3] Itzhack Y Bar-Itzhack and Richard R Harman. Optimized triad algorithm for attitude determination. *Journal of guidance, control, and dynamics*, 20(1):208–211, 1997.

[4] Andrea Colagrossi and Michèle Lavagna. Fully magnetic attitude control subsystem for picosat platforms. *Advances in Space Research*, 2017.

[5] Juan M Fernandez, Lourens Visagie, Mark Schenk, Olive R Stohlman, Guglielmo S Aglietti, Vaios J Lappas, and Sven Erb. Design and development of a gossamer sail system for deorbiting in low earth orbit. *Acta Astronautica*, 103:204–225, 2014.

[6] Bo Fu, Evan Sperber, and Fidelis Eke. Solar sail technology—a state of the art review. *Progress in Aerospace Sciences*, 86:1–19, 2016.

[7] Torkel Glad and Lennart Ljung. *Control theory*. CRC press, 2014.

[8] JT Grundmann, P Spietz, P Seefeldt, and T Spröwitz. Gossamer deployment systems for flexible photovoltaics. In *67th International Astronautical Congress*, 2016.

[9] Jose Luis Redondo Gutierrez. Attitude control of flexible spacecraft attitude control of flexible spacecraft. Master's thesis, TU Delft, 2019.

[10] I Harris and W Priester. Relation between theoretical and observational models of the upper atmosphere. *Journal of Geophysical Research*, 68(20):5891–5894, 1963.

[11] Jack B Kuipers et al. *Quaternions and rotation sequences*, volume 66. Princeton university press Princeton, 1999.

[12] Patric Seefeldt, Peter Spietz, Tom Sproewitz, Jan Thimo Grundmann, Martin Hillebrandt, Catherin Hobbie, Michael Ruffer, Marco Straubel, Norbert Tóth, and Martin Zander. Gossamer-1: Mission concept and technology for a controlled deployment of gossamer spacecraft. *Advances in Space Research*, 59(1):434–456, 2017.

[13] Thomas Sinn, L Tiedemann, A Riemer, R Hahn, et al. Results of the deployable membrane & adeo passive de-orbit subsystem activities leading to a dragsail demonstrator. In *7th European Conference on Space Debris*, 2017.

[14] Jan Thimo Grundmann Frederik Haack Martin Hillebrandt Hauke Martens Sebastian Meyer Siebo Reershemius Nies Reininghaus Kaname Sasaki Patric Seefeldt Oleg Sergeev · Peter Spietz Maciej Sznajder Norbert Toth Martin Vehse Torben Wippermann Martin E. Zander Tom Sproewitz, Udayan Banik. Concept for a gossamer solar power array using thin film photovoltaics. *CEAS Space Journal*, 2019.

[15] Yuichi Tsuda, Osamu Mori, Ryu Funase, Hirotaka Sawada, Takayuki Yamamoto, Takanao Saiki, Tatsuya Endo, Katsuhide Yonekura, Hirokazu Hoshino, and Jun'ichiro Kawaguchi. Achievement of IKAROS - Japanese deep space solar sail demonstration mission. *Acta Astronautica*, 82(2):183–188, 2013.

[16] Firdaus E. Udwadia and Robert E. Kalaba. *Analytical Dynamics: A New Approach*. Cambridge University Press, 1996.

[17] Firdaus E Udwadia and Harshavardhan Mylapilli. Constrained motion of mechanical systems and tracking control of nonlinear systems: connections and closed-form results. *Nonlinear Dyn. Syst. Theory*, 15(1):73–89, 2015.

[18] James R Wertz. *Spacecraft attitude determination and control*, volume 73. Springer Science & Business Media, 2012.

[19] Bong Wie, David Murphy, Michael Paluszek, and Stephanie Thomas. Robust attitude control systems design for solar sails (part 1): Propellantless primary acs. In *AIAA Guidance, Navigation, and Control Conference and Exhibit*, page 5010, 2004.

7. Appendix

7.1 *Satellite's data*

The GoSolAr satellite has two structural configuration: stowed (S) and deployed (D). In the deployed configuration it consists of a central rigid body to which 4 booms are attached and a solar array fixed to the central body and the tip of the booms (figure2). In the stowed configuration all this structure is stored inside the central body. Table 1 contains structural properties and table 2 the mass properties of the satellite.

Property [units]	Magnitude	Property [units]	Magnitude
Dimensions(S) $[m^3]$	0.5x0.5x0.5	Membrane area $[m^2]$	25
Boom length $[m]$	3.5355		

Table 1: Geometrical data.

Property [units]	Magnitude	Property [units]	Magnitude
Stowed mass $[kg]$	60.8	Membrane mass $[kg]$	6.2
Central part mass $[kg]$	53.1	Boom mass $[kg]$	0.38
Ixx(S) $[kgm^2]$	3.19	Ixx(D) $[kgm^2]$	17.3130
Iyy(S) $[kgm^2]$	3.42	Iyy(D) $[kgm^2]$	18.9068
Izz(S) $[kgm^2]$	2.92	Izz(D) $[kgm^2]$	31.7930
Ixy(S) $[kgm^2]$	0.005	Ixy(D) $[kgm^2]$	0.005
Ixz(S) $[kgm^2]$	-0.01	Ixz(D) $[kgm^2]$	-0.01
Iyz(S) $[kgm^2]$	-0.011	Iyz(D) $[kgm^2]$	-0.004
CoG(S) $[m]$	[0 0 0]	CoG(D) $[m]$	[0 0 0.05]

Table 2: Mass data.

Additional properties that needs to be considered but are not related to structural and mass properties are:

Property [units]	Magnitude	Property [units]	Magnitude
C_D (drag coefficient) [-]	1.2	Magnetic dipole module $[Am^2]$	0.1
Spectral reflectance coefficient[-]	0.5	Diffuse reflectance coefficient [-]	0.5

Table 3: Interaction of the satellite with the environment.

7.2 *Magnetorquer specifications*

The properties of the magnetic torque bars are shown in table 4.

Actuator	Property [units]	Magnitude
Magnetorquer	Max dipole $[Am^2]$	10
Magnetorquer	Time constant $[s]$	0.05
Magnetorquer	Duty cycle [%],[s]	90%, 5

Table 4: Actuator specifications.